The Cryosphere
Discussions

Annual Greenland accumulation rates (2009–2012) from airborne Snow Radar

L. S. Koenig[1], A. Ivanoff[2], P. M. Alexander[3,4], J. A. MacGregor[5], X. Fettweis[6], B. Panzer[7], J. D. Paden[7], R. R. Forster[8], I. Das[9], J. McConnell[10], M. Tedesco[4,9], C. Leuschen[7], and P. Gogineni[7]

[1]National Snow and Ice Data Center, University of Colorado, Boulder, CO, USA
[2]ADNET Systems, Inc., Bethesda, MD, USA
[3]NASA Goddard Institute for Space Studies, New York, NY, USA
[4]City College of New York, New York, NY, USA
[5]Institute for Geophysics, The University of Texas at Austin, Austin, TX, USA
[6]Department of Geography, University of Liège, Belgium
[7]Center for Remote Sensing of Ice Sheets, University of Kansas, Lawrence, KS, USA
[8]Department of Geography, University of Utah, Salt Lake City, UT, USA
[9]Lamont-Doherty Earth Observatory, Columbia University, New York, NY, USA
[10]Division of Hydrologic Science, Desert Research Institute, NV, USA

6697

Abstract

Contemporary climate warming over the Arctic is accelerating mass loss from the Greenland Ice Sheet (GrIS) through increasing surface melt, emphasizing the need to closely monitor surface mass balance (SMB) in order to improve sea-level rise predictions. Here, we quantify accumulation rates, the largest component of GrIS SMB, at a higher spatial resolution than currently available, using Snow Radar stratigraphy. We use a semi-automated method to derive annual-net accumulation rates from airborne Snow Radar data collected by NASA's Operation IceBridge from 2009 to 2012. An initial comparison of the accumulation rates from the Snow Radar and the outputs of a regional climate model (MAR) shows that, in general, the radar-derived accumulation matches closely with MAR in the interior of the ice sheet but MAR estimates are high over the southeast GrIS. Comparing the radar-derived accumulation with contemporaneous ice cores reveals that the radar captures the annual and long-term mean. The radar-derived accumulation rates resolve large-scale patterns across the GrIS with uncertainties of up to 11 %, attributed mostly to uncertainty in the snow/firn density profile.

1 Introduction

Contemporary climate warming over the Greenland Ice Sheet (GrIS) has accelerated its mass loss, nearly quadrupling from $\sim 55\,\mathrm{Gt\,yr^{-1}}$ between 1993–99 (Krabill et al., 2004) to $\sim 210\,\mathrm{Gt\,yr^{-1}}$ of ice, equivalent to $\sim 0.6\,\mathrm{mm\,yr^{-1}}$ of sea level rise, between 2003–08 (Shepherd et al., 2012). As GrIS mass loss has accelerated, a fundamental change in the nature of this loss has occurred. The dominant mass loss process for the GrIS is changing from being governed by ice dynamics to being dominated by surface mass balance (SMB) processes (van den Broeke, 2009; Enderlin et al., 2014). This recent shift emphasizes the need to monitor SMB which, over most of the GrIS, is dominated by net accumulation.

Here we use the complete set of airborne Snow Radar data collected by NASA's Operation IceBridge (OIB) over the GrIS from 2009 to 2012 to produce annual-net accumulation rates, here after called accumulation for simplicity, along those flightlines. The radar-derived accumulation rates are compared to both in situ data and model outputs from the Modèle Atmosphérique Régional (MAR).

2 Background

In situ accumulation-rate measurements are limited by the time and cost of acquiring ice cores, digging snow pits or monitoring stake measurements across large sectors of the ice sheet. Only two major accumulation-rate measurement campaigns have been undertaken across the GrIS, the first in the 1950's when the US Army collected pit data along long traverse routes (Benson, 1962) and the second in the 1990's when the Program on Arctic and Regional Climate Assessment (PARCA) collected an extensively distributed set of ice cores (e.g. Mosley-Thompson et al., 2001). A recent traverse and study by Hawley et al. (2014) reports a 10 % increase in accumulation since the 1950's and highlights the need to monitor how Greenland precipitation is evolving in the midst of ongoing climate change. Although many other accumulation-rate measurements exist, they are more limited in either space or time (e.g. Dibb and Fahnestock, 2004; Hawley et al., 2014).

To date there is no annually resolved satellite-retrieval algorithm for accumulation rate across ice sheets. Hence, the two primary methods used to generate large-scale (hundreds of km) accumulation-rate patterns are model predictions and radar-derived accumulation rates (Koenig et al., 2015). High resolution, near-surface radar data have shown good fidelity at mapping spatial patterns of accumulation over ice sheets at decadal and annual resolutions from both airborne and ground-based radars (Kanagaratnam et al., 2001, 2004; Spikes et al., 2004; Arcone et al., 2005; Anshütz et al., 2008; Müller et al., 2010; Medley et al., 2013; Hawley et al., 2006, 2014; de la Peña et al., 2010; Miège et al., 2013). Radars detect and map isochronal layers within the

firn. When these layers are either (1) dated in conjunction with ice cores or (2) annually resolved from the surface, they can be used to determine along-track accumulation rates.

Early studies by Spikes et al. (2004) in Antarctica and Kanagaratnam et al. (2001 and 2004) in Greenland used high/very high-frequency (100 to 1000 MHz) ground-based and airborne radars, with vertical resolutions of ∼ 30 cm, to monitor decadal-scale accumulation rates between dated ice cores. These high/very high-frequency radars can penetrate to hundreds of meters in the dry-snow zone and tens of meters in the ablation zone (Kanagaratnam et al., 2004). Subsequent studies utilized the larger bandwidths of ultra/super-high frequency (2 to 20 GHz), frequency-modulated continuous wave (FMCW) radars, with centimeter-scale vertical resolutions capable of mapping annual layers within ice sheets (e.g. Legarsky, 1999; Marshall and Koh, 2008; Medley et al., 2013). Ultra/super-high frequency radars can penetrate tens of meters in the dry-snow zone and meters in the ablation zone. Legarsky (1999) was among the first to show that such radars could image annual layers, and Hawley et al. (2006) further demonstrated that a 13.2 GHz (Ku-band) airborne radar imaged annual layers in the dry-snow zone of the GrIS to depths of up to 12 m.

Most previous studies used radar data that overlapped spatially with ice cores or snow pits for both dating layers and density information. Medley et al. (2013) and Das et al. (2015), however, showed that accumulation rates could be derived using density from a regional ice core ensemble. The end members of density are used as the uncertainty limits and the derived regional density profile is sufficient for radar studies of accumulation and SMB (Das et al., 2015). Additionally, Medley et al. (2013) showed that the Snow Radar was capable of resolving annual layering in high accumulation regions where the layers were preserved and, therefore, it was possible to date the layers by counting from the surface downwards.

Regional and Global Climate Models (RCMs and GCMs) and reanalysis products provide the only spatially and temporally extensive estimates of accumulation-rate fields at ice-sheet scales (e.g. Burgess et al., 2010; Hanna et al., 2011; Ettema et al.,

2009; Fettweis, 2007; Cullather et al., 2014). In a comprehensive model intercomparison study, Vernon et al. (2013) found that modelled accumulation rates had the least spread across RCM's but still had a ∼ 20 % variance. Chen et al. (2011) found the range in average accumulation across the GrIS between 5 reanalysis models to be ∼ 15 to 30 cm yr^{-1}, while Cullather and Bosilovich (2011) found the range in average accumulation across the GrIS between reanalysis data and RCM's to be ∼ 34 to 42 cm yr^{-1}. Overall, while these models continue to improve, there is clearly a continuing need for large-scale accumulation-rate measurements to evaluate their outputs.

3 Data, instruments and model description

3.1 Snow radar and data

Annual layers in the GrIS snow/firn were mapped using the University of Kansas' Center for Remote Sensing of Ice Sheets (CReSIS) ultra-wideband Snow Radar during NASA's Operation IceBridge (OIB) Arctic Campaigns from 2009 through 2012 (Leuschen, 2014). The radar operates over the frequency range from ∼ 2 to 6.5 GHz (Panzer et al., 2013; Rodriguez-Morales et al., 2014). The Snow Radar uses a Frequency-Modulated Continuous Wave (FMCW) design to provide a vertical-range resolution of ∼ 4 cm in snow/firn, capable of resolving annual layering, when preserved, to tens of meters in depth (Medley et al., 2013).

3.2 Modelled accumulation rates and density

Accumulation rate and snow/firn density profiles were derived from the MAR RCM (v3.5.2; X. Fettweis, personal communication, 2015). MAR is a coupled surface–atmosphere model that simulates fluxes of mass and energy in the atmosphere and between the atmosphere and the surface in three dimensions, and is forced at the lateral boundaries with climate reanalysis outputs (Gallée, 1997; Gallée and Schayes, 1994; Lefebre et al., 2003). It incorporates the atmospheric model of Gallée and Schayes

(1994), and the Soil Ice Snow Vegetation Atmosphere Transfer scheme (SISVAT) land surface model, which includes the multi-layer Crocus snow model of Brun et al. (1992). The MAR v3.5.2 simulation used here utilizes reanalysis outputs from the European Center for Medium Range Weather Forecasting (ECMWF) ERA-Interim (Dee et al., 2011) at the lateral boundaries, with a horizontal resolution of 25 km. The details of this setup are described further by Fettweis (2007), with further updates described by Fettweis et al. (2011, 2013) and Alexander et al. (2014). MAR has been validated with in situ data and remote sensing data over GrIS, including data from weather stations (e.g. Lefebre et al., 2003; Fettweis et al., 2011), in situ and remote sensing albedo data (Alexander et al., 2014), and ice-core accumulation-rate estimates (Colgan et al., 2015), and it has been used to model both past and future SMB (Fettweis et al., 2005, 2013). We use accumulation-rate and density profiles simulated by MAR for the period during which the radar data were collected (2009 to 2012).

3.3 In situ density and accumulation data

The SUrface Mass balance and snow depth on sea ice working group (SUMup) dataset (July 2015 release) contains a compilation of publically available accumulation, snow depth and density measurements over both sea ice and ice sheets (Koenig et al., 2012). We use two subsets of this data. First, to characterize density across the GrIS, we extract the snow/firn density measurements ranging in depth from the snow surface to 15 m (the depth to which MAR predicts firn densities), which contains over 1500 measurements from snow pits and ice cores (Koenig et al., 2015, 2014; Miège et al., 2013; Mosley-Thompson et al., 2001; Hawley et al., 2014; Baker, 2015) (Fig. 1). Second, to compare radar-derived and measured accumulation rates, we consider only accumulation-rate measurements within 5 km of OIB Snow Radar data, a criterion that includes 11 ice cores from the SUMup dataset (Mosley-Thompson et al., 2001). To expand this comparison, an additionally dataset of 71 ice cores (J. McConnell, personal communication, 2015) which includes additional cores to the SUMup dataset,

was used to locate accumulation measurements within 5 km of OIB Snow Radar data providing 23 additional ice cores (Fig. 1).

4 Methods

4.1 Determining the density profile and uncertainties

Because we seek to derive accumulation rates from near-surface radars across large portions of the ice sheet, we require firn density profiles that cover and vary across the GrIS. Modelled snow/firn density profiles from the MAR model were investigated for use. However, a preliminary comparison of the SUMup-measured density profiles to MAR-estimated density profiles showed that MAR simulated density values in the top 1 m of snow/firn were significantly lower ($0.284 \pm 0.050\,\mathrm{g\,cm^{-3}}$) than observed ($0.338 \pm 0.039\,\mathrm{g\,cm^{-3}}$) (Fig. 2). We consider it beyond the scope of this study to investigate and explain why MAR underestimates near-surface density, therefore, here we assume that the firn density in the top 1 m is $0.338\,\mathrm{g\,cm^{-3}}$. Below 1 m, the model and observed densities are similar (4 % mean difference), so the spatially-varying modelled density profiles are used. Hence, a hybrid measured-modelled density profile is used to determine accumulation rates from the snow radar data (Fig. 2).

Uncertainty in the top meter is assigned by the $\pm 1\sigma$ variation in observed density (12 %). We note that this uncertainty is broadly consistent with that which we expect due to natural variability in surface density across the GrIS. This natural variation, however, represents a smaller assumed error than the mean difference between the modelled and observed values within the top 1 m (16 %).

4.2 Deriving accumulation rates from Snow Radar and uncertainties

The radar travel time is converted to depth (z) using the snow/firn density profile and the dielectric mixing model of Looyenga (1965). Possible errors in radar-derived depth

come from two sources: (1) the dielectric mixing model chosen and (2) layer picking. The choice of the dielectric mixing model maximizes potential error at a density of $\sim 0.300\,\mathrm{g\,cm^{-3}}$. The maximum possible difference in depth over 15 m is 3 % assuming a constant density of $0.320\,\mathrm{g\,cm^{-3}}$ and < 1 % assuming a constant density of $0.600\,\mathrm{g\,cm^{-3}}$ (Wiesmann and Matzler, 1999; Gubler and Hiller, 1984; Schneebeli et al., 1998; Looyenga, 1965; Tiuri et al., 1984). The second source of error occurs during manual adjustment of the picked layers (Sect. 4.3.4) and is estimated to be ±3 bins or $\sim 8\,\mathrm{cm}$.

Accumulation rate is derived using the standard equation for converting depth from a radar profile to accumulation rates at location (x):

$$\dot{b}(x) = \frac{\mathrm{TWT}(x)\rho(x)c}{2a(x)\rho_w \left(\frac{\rho(x)}{\rho_i}\left(\epsilon_i'^{1/3} - 1\right) + 1\right)^{3/2}} \qquad (1)$$

Where $\dot{b}$ is water equivalent accumulation rate in m w.e. $\mathrm{yr^{-1}}$, TWT is the two-way travel time to the dated layer in sec, ρ is cumulated snow/firn density at that depth in $\mathrm{kg\,m^{-3}}$, c is the speed of light in $\mathrm{m\,s^{-3}}$, a is age of the layer in years from the date of radar data collection, ρ_w is water density in $\mathrm{kg\,m^{-3}}$, ρ_i is ice density in $\mathrm{kg\,m^{-3}}$ and ε_i' is the dielectric permittivity of ice. The cumulative snow/firn density (ρ) is determined by the density profile previously described in Sect. 4.1. The layers are picked in the radar data using a semi-automated approach (Sect. 4.3).

Layer ages are determined by assuming spatially continuous layers are annually resolved and dated accordingly from the year the radar data were collected. The radar data were collected during springtime (April–May) and the surface is assumed to be 30 April. The picked layers at depth are assumed to be 1 July ± 1 month as follows. A peak in radar reflection, assuming ice with no impurities, is caused by the largest change in snow density. In the ablation and percolation zone, the peak in density difference occurs in the summer between the snow layer and ice or the snow/firn layer and the high-density melt/crust layer, respectively (e.g. Nghiem et al., 2005). In the dry snow

6705

zone, the peak in density difference also occurs in the summer between the summer hoar layer and the denser snow/firn layer (e.g. Alley et al., 1990).

To calculate the total uncertainty on the radar-derived accumulation rate, the maximum error is assumed for both density (12 %) and age (8 %). Equation (1) is written to show the relationship between the density profile, which is used both for calculating depth and water equivalent. The derivative of Eq. (1) is used to determine the correlated error between depth and density. Assuming uncorrelated and normally distributed errors between density and age, the maximum accumulation-rate uncertainty is 11 %, with uncertainty in the density profile in the top meter of firn being the largest contributor. Uncertainty from our study is very similar to studies by Medley et al. (2013) and Das et al. (2015) for radar-derived accumulation rates.

4.3 Semi-automated radar layer picker

A semi-automated layer detection algorithm was developed to process the large amounts of radar data gathered by OIB ($> 10^4\,\mathrm{km\,yr^{-1}}$), analogous to the challenges faced by MacGregor et al. (2015) for analysis of very high frequency "deep" radar data. A previously developed semi-automated method designed by Onana et al. (2014) was tested for this application but proved too computationally intensive, with higher error rates than the method described here. While a fully automated method is ultimately desirable, we have found that it is necessary to manually check every automated pick, making adjustments as needed by an experienced analyst, to distinguish between spatially discontinuous radar reflectors, caused by the normal heterogeneity of firn microstructure, and spatially consistent annual layers. The algorithm processes the OIB Snow Radar data in four steps outlined below.

4.3.1 Surface alignment

The snow surface is detected by a threshold, set to four times the mean radar return from air, which is assumed to be the radar noise level. A median filter is applied ver-

6706

tically to each radar trace to minimize data noise. In addition, any surface value that exceeds a distance threshold of 10 range bins ($\sim 25\,cm$) from its neighbors is not used and that entire vertical trace is ignored in subsequent analysis. Data arrays are then aligned to the surface and truncated above and below the surface (200 and 800 range bins, respectively), equivalent to $\sim 25\,m$ into the snow/firn, to reduce data volumes. Layer depths are measured relative to the snow surface. The radar data are then horizontally averaged (stacked) to an along-track spacing of $\sim 50\,m$, in 2011 and 2012, and $\sim 10\,m$, in 2009 and 2010, and split into equally sized sections of 2000 traces per radargram for easier processing.

4.3.2 Layer detection

The algorithm takes advantage of the difference between high-frequency and low-frequency spatial variability to identify peaks in returned power in the radar data. Peaks are formed by the stratified accumulation layers, resulting in density changes, which extend across the GrIS. The point at which the peak forms occurs over a small spatial scale, or at a high frequency. The peak detection process is thus a type of high-pass filter, resulting in the set of disjointed points in adjacent traces along the flight path. These points are stored as layer segments using the half maximum width of the peak's waveform, resulting in continuous layer segments over the radar data profile (Fig. 3).

4.3.3 Layer indexing

Each detected layer is indexed, with both a number and the corresponding year (Fig. 3). This process is accomplished by indexing the layers downward from the surface. The indexing process begins with the segmentation of the layers, so that each layer is uniquely identifiable. The peak points within each segment are then connected by smoothed spline fits, resulting in a set of sharply defined layers. Layer indices are assigned from top to bottom to take into account the partial overlap that can exist between layers.

4.3.4 Manual adjustment with the Layer Editor

A graphical user interface (GUI) was developed to verify the automated layer detections. An analyst used the GUI to quickly compare the picked layers and the radargram. The GUI application allows for editing of the output layers as needed.

5 Results

5.1 Radar-derived accumulation rates over the GrIS

Annual radar-derived accumulation rates and their uncertainties were calculated for all 2009–2012 OIB radar data that contained detected layers (Fig. 4). The increase in coverage from 2009 to 2012 is related to an increasing number of OIB flights over the GrIS and adjustments to the Snow Radar antenna and operations that improved overall data quality. These accumulation-rate patterns are consistent with observed and modelled large-scale spatial patterns for the GrIS: high accumulation rates in the southeast-coastal sector and lower accumulation rates in the northeast (Fig. 5). Year-to-year variability in accumulation rate is also evident and can be seen even at the ice-sheet scale, e.g., in the southeast accumulation rates were lower in 2010 than in 2011.

The radar-derived accumulation in Fig. 4 represents only the first layer detected by the Snow Radar, or approximately the annual accumulation rate from the year prior to data collection. For simplicity, we refer to this quantity as the annual accumulation rate, but we caution that it does not strictly represent the calendar year. The values shown in Fig. 4 represent only 10 months of accumulation, based on our assumption that the radar layers date to 1 July (Sect. 4.2) and that the data collection date is 30 April for all OIB data. When comparing the first layer of radar-derived accumulation to modelled estimates from MAR (Fig. 5) or other accumulation measurements, this

Discussion Paper | Discussion Paper | Discussion Paper | Discussion Paper |

timing difference must be considered. Although the first layer represents only a partial year, all deeper layers represent a full year, from 1 July to 30 June.

Figure 6 shows the number of detected layers, or previous years, discernable in the OIB radar data. For the majority of the GrIS, 1 to 3 annual layers are discernable, due to the spatial distribution of OIB flightlines. OIB flightlines are clustered in the ablation/percolation zones of the GrIS, where radar penetration depths are reduced by the increased density, englacial water and layering structure of the firn column (Fig. 3). In the GrIS interior, where dry snow conditions allow deeper radar penetration, annual layering going back over two decades is detectable (Fig. 3).

Crossover points were assessed to determine the internal consistency of the radar-derived accumulation rates (Figs. 7 and 8). While no consistent spatial pattern is found in the crossover errors, the largest discrepancies were found in 2011 and 2012 in the northwest and southeast (Fig. 7). Other inconsistencies are likely due to snow storms occurring between flights in the southeast and incorrectly picked layers that were either sub- or multi-annual in the northwest. Figure 8 shows a scatterplot of crossover points. There are relatively few outliers, and those that are outlying are generally offset by a factor of two, suggesting an error in layer detection/dating rather than a radar-system error. Crossover differences per year, including the mean, standard deviation and maximum, are listed in Table 1. Crossover differences are comparable (mean of 0.04 m w.e.) to our inferred relative uncertainty of 11 % which emphasizes the overall validity of our chosen methods.

5.2 Comparison with modelled accumulation

The radar-derived accumulation rate was gridded to the MAR grid for comparison. The mean-local, radar-derived accumulation rate was used when gridding. Because OIB flightlines are not spatially heterogeneous, each MAR grid cell represents a different number of radar-derived values, so grid cells are not sampled equally. With this discrepancy noted, this gridding method is still the most straightforward and useful approach for this comparison. Figure 9 shows the difference between the radar-derived

and MAR accumulation rates. The mean difference for all years is low (0.02 m w.e.). Table 1 shows the annual variability of the mean difference, which is low for every year except 2010, when large differences are seen over the southeast coastal region of the GrIS (Fig. 9).

Figure 9 shows that MAR generally predicts accumulation well in the GrIS interior (consistent with the comparison with ice core estimates presented by Colgan et al., 2015), but has larger errors around the periphery, especially in the southeast and northwest. In the southeast, MAR generally overestimates accumulation rates, except in 2011 when there is a mixed pattern of agreement and overestimation. This pattern of overestimation in the southeast is not surprising and is likely due to the lack of previous measurements in the region to constrain accumulation and the large changes in surface topography that are not resolved by the relatively large grid size used in modelled estimates (Burgess et al., 2010). In 2011, the northwest coastal region of the GrIS was well sampled by OIB and MAR shows an underestimation of accumulation rate, but the origin of this anomaly is less clear.

Figure 10 shows a scatterplot of the radar-derived and MAR-estimated accumulation rates. These values are not well correlated (Pearson correlation coefficient $r^2 = 0.2$) and have large RMSE (0.24 m w.e.), emphasizing that further improvements in accumulation-rate modeling are needed, particularly over the southeast and northwest GrIS.

5.3 Comparison with annually resolved in situ data

Between 2009 and 2012, OIB flew within 5 km of 34 ice-core locations but only two locations, NEEM and Camp Century (Fig. 1) were coincident in time with the layers we detected. Each of these locations has two cores, providing annual accumulation rates and a measure of spatial variability. Figure 11 compares the radar-derived to ice-core measured accumulation rates. At NEEM, the two ice cores and radar data are closely located, within 0.6 km of each other. The radar-derived accumulation rates are self-consistent between 2011 and 2012 and agree well with the ice cores (Root

Mean Square Error (RMSE) of 0.06 m w.e.). For comparison, the two NEEM ice cores have a RMSE of 0.05 m w.e. for the period of overlap. A timing discrepancy arises with this comparison because the ice cores, with higher dating resolution from isotopic and chemical analysis, are dated and reported as the calendar year, whereas as the radar-derived accumulation is assumed 30 June–1 July (Sect. 4.2). This mismatch in the measurement is likely evident in Fig. 11 by the differences in the annual peaks between the cores and radar-derived accumulation having similar means yet differing magnitudes from year to year.

Near Camp Century, the ice cores and radar data are farther apart from each other. The radar-data are located within 4.4 km of the Camp Century core and the GITS core is located ~ 8.2 km from the Camp Century core. These separations are likely responsible for the poorer agreement at this site of radar-derived accumulation rate to the Camp Century core (RMSE 0.10 m w.e.) and the larger difference (RMSE 0.07 m w.e.) in accumulation rate between the two cores for the period of overlap. While it is more difficult to analyze the results at Camp Century, with only 3 points of overlap and no time series of radar-derived accumulation, it is evident that the radar-derived accumulation rates are within the expected variability and capture the long-term mean value.

6 Discussion

This study is the first to derive annual accumulation rates from near-surface airborne radar data collected across the large portions of the GrIS. The pattern of radar-derived accumulation rates compares well with known large-scale patterns and clearly shows that these accumulation-rate measurements are useful for evaluating model estimates. At the two locations with contemporaneous cores, the radar-derived rates agree well with the long-term mean. Additional cores, with direct overflights, are clearly needed to continue assessing the accuracy of the radar-derived accumulation rates from the layers within the firn over the GrIS.

The work shown here only incorporates layering detected in the radar data that is annual and continuous from the surface to depth. It does not exhaust all layering detected by the Snow Radar, i.e., there are still contiguous layers in the dataset that were not utilized. For example, in the central-northern GrIS, there is a strongly reflecting layer varying between 15 and 18 m that cannot be dated with the radar data alone. If ice cores were drilled to identify this layer, techniques similar to those developed by MacGregor et al. (2015) or Das et al. (2015) could be used to determine multi-annual accumulation rates in additional regions of the GrIS. Additionally, further deconvolution processing of the radar data, currently ongoing at CReSIS, resolves additional deep layers in the Snow Radar data that will expand accumulation measurements in the future.

Annual-radar-derived accumulation rates are not extrapolated spatially here. Spatial extrapolation between the constantly varying flightlines will be left for future work, as additional data are collected and made available to fill in gaps.

Finally, the largest uncertainty in the radar-derived accumulation rate comes from the hybrid measured-modelled density profiles used. Spatially distributed density measurements and improved density models spanning the entire firn column are required to take full advantage of the layering detected by near-surface radars and to reduce the errors in radar-derived accumulation rates. More specifically, as shown in Fig. 1, the current sampling of measurements has large spatial gaps over the southwestern and northeastern GrIS and the majority of the measurements are located in the upper-percolation and dry-snow zones. To further constrain and improve density models required for radar-derived accumulation rates, these spatial gaps and sampling distributions need to be filled to broaden with additional measurements.

7 Conclusions

A semi-automated method was developed to process tens of thousands of kilometers of airborne Snow Radar data collected by OIB across the GrIS between 2009 and

2012. The resulting radar-derived accumulation dataset represents the largest validation dataset for recent annual accumulation across the GrIS to date. This dataset captures the large-scale accumulation-rate patterns of the GrIS well. Over two decades of annual radiostratigraphy is observed in the dry snow zone, near Summit Station, and 1 to 3 years are generally detectable in the ablation/percolation zones. Our estimated uncertainty in the radar-derived accumulation is 11 %, with the largest error contribution coming from the hybrid measured-modelled density profiles. This study emphasizes the need for ice cores coincident in time with airborne overflights and, more importantly, for improved density profiles, particularly in the top 1 m of snow/firn. These radar-derived accumulation-rate datasets should be used to evaluate RCM/GCM and reanalysis products, as demonstrated here using the MAR model. MAR reproduces the radar-derived accumulation rates for most of the interior of the GrIS, but tends to overestimate accumulation rates in the southeastern coastal region of the GrIS and, in at least one year, underestimates accumulation rates in the northwestern costal region of the GrIS. While determining the precise nature of these differences is left for future work, we have clearly demonstrated the usefulness of the ice-sheet-wide, radar-derived accumulation-rate datasets for improving SMB estimates. As the GrIS continues to lose mass through SMB processes, monitoring accumulation rates directly is vital.

References

Alexander, P. M., Tedesco, M., Fettweis, X., van de Wal, R. S. W., Smeets, C. J. P. P., and van den Broeke, M. R.: Assessing spatio-temporal variability and trends in modelled and measured Greenland Ice Sheet albedo (2000–2013), The Cryosphere, 8, 2293–2312, doi:10.5194/tc-8-2293-2014, 2014.

Alley, R. B., Saltzman, E. S., Cuffey, K. M., and Fitzpatrick, J. J.: Summertime formation of Depth Hoar in central Greenland, Geophys. Res. Lett., 17, 2393–2396, doi:10.1029/GL017i013p02393, 1990.

Anschütz, H., Steinhage, D., Eisen, O., Oerter, H., Horwath, M., and Ruth, U.: Small-scale spatio-temporal characteristics of accumulation rates in western Dronning Maud Land, Antarctica, J. Glaciol., 54, 315–323, doi:10.3189/002214308784886243, 2008.

Arcone, S. A., Spikes, V. B., and Hamilton, G. S.: Phase structure of radar stratigraphic horizons within Antarctic firn, Ann. Glaciol., 41, 10–16, doi:10.3189/172756405781813267, 2005.

Benson, C. S.: Stratigraphic studies in the snow and firn of the Greenland Ice sheet, SIPRE Res. Rep., 70, 1–89, 1962.

Baker, I.: Density and permeability measurements with depth for the NEEM 2009S2 firn core, ACADIS Gateway, https://www.aoncadis.org/dataset/neem_firn_core_2009s2_density_and_permeability.html, 2015.

Brun, E., David, P., Sudul, M., and Brunot, G.: A numerical model to simulate snow-cover stratigraphy for operational avalanche forecasting, J. Glaciol., 38, 13–22, 1992.

Burgess, E. W., Forster, R. R., Box, J. E., Mosley-Thompson, E., Bromwich, D. H., Bales, R. C., and Smith, L. C.: A spatially calibrated model of annual accumulation rate on the Greenland Ice Sheet (1958–2007), J. Geophys. Res., 115, F02004, doi:10.1029/2009JF001293, 2010.

Chen, L., Johannessen, O. M., Wang, H., and Ohmura, A.: Accumulation over the Greenland Ice Sheet as represented in reanalysis data, Adv. Atmos. Sci., 28, 1030–1038, doi:10.1007/s00376-010-0150-9, 2011.

Colgan, W., Box, J. E., Andersen, M. L., Fettweis, X., Csathó, B., Fausto, R. S., Van As, D., and Wahr, J.: Greenland high-elevation mass balance: inference and implication of reference period (1961–90) imbalance, Ann. Glaciol., 56, 105–117, doi:10.3189/2015AoG70A967, 2015.

Cullather, R. I. and Bosilovich, M. G.: The Energy Budget of the Polar Atmosphere in MERRA, J. Climate, 25, 5–24, doi:10.1175/2011JCLI4138.1, 2012.

Cullather, R. I., Nowicki, S. M., Zhao, B., and Suarez, M. J.: Evaluation of the surface representation of the Greenland Ice Sheet in a general circulation model, J. Climate, 27, 4835–4856, 2014.

Das, I., Scambos, T. A., Koenig, L. S., van den Broeke, M. R., and Lenaerts, J. T. M.: Extreme wind-ice interaction over Recovery Ice Stream, East Antarctica, Geophys. Res. Lett., 42, 2015GL065544, doi:10.1002/2015GL065544, 2015.

Dee, D. P., Uppala, S. M., Simmons, A. J., Berrisford, P., Poli, P., Kobayashi, S., Andrae, U., Balmaseda, M. A., Balsamo, G., Bauer, P., Bechtold, P., Beljaars, A. C. M., van de Berg, L., Bidlot, J., Bormann, N., Delsol, C., Dragani, R., Fuentes, M., Geer, A. J., Haimberger, L., Healy, S. B., Hersbach, H., Hólm, E. V., Isaksen, L., Kållberg, P., Köhler, M., Matricardi, M., McNally, A. P., Monge-Sanz, B. M., Morcrette, J.-J., Park, B.-K., Peubey, C., de Rosnay, P., Tavolato, C., Thépaut, J.-N., and Vitart, F.: The ERA-Interim reanalysis: configuration and performance of the data assimilation system, Q. J. Roy. Meteor. Soc., 137, 553–597, doi:10.1002/qj.828, 2011.

de la Peña, S., Nienow, P., Shepherd, A., Helm, V., Mair, D., Hanna, E., Huybrechts, P., Guo, Q., Cullen, R., and Wingham, D.: Spatially extensive estimates of annual accumulation in the dry snow zone of the Greenland Ice Sheet determined from radar altimetry, The Cryosphere, 4, 467–474, doi:10.5194/tc-4-467-2010, 2010.

Dibb, J. E. and Fahnestock, M.: Snow accumulation, surface height change, and firn densification at Summit, Greenland: insights from 2 years of in situ observation, J. Geophys. Res., 109, D24113, doi:10.1029/2003JD004300, 2004.

Enderlin, E. M., Howat, I. M., Jeong, S., Noh, M.-J., van Angelen, J. H., and van den Broeke, M. R.: An improved mass budget for the Greenland ice sheet, Geophys. Res. Lett., 41, 2013GL059010, doi:10.1002/2013GL059010, 2014.

Ettema, J., van den Broeke, M. R., van Meijgaard, E., van de Berg, W. J., Bamber, J. L., Box, J. E., and Bales, R. C.: Higher surface mass balance of the Greenland ice sheet revealed by high-resolution climate modeling, Geophys. Res. Lett., 36, L12501, doi:10.1029/2009GL038110, 2009.

Fettweis, X.: Reconstruction of the 1979–2006 Greenland ice sheet surface mass balance using the regional climate model MAR, The Cryosphere, 1, 21–40, doi:10.5194/tc-1-21-2007, 2007.

Fettweis, X., Gallée, H., Lefebre, F., and Ypersele, J.-P. van: Greenland surface mass balance simulated by a regional climate model and comparison with satellite-derived data in 1990–1991, Clim. Dynam., 24, 623–640, doi:10.1007/s00382-005-0010-y, 2005.

Fettweis, X., Tedesco, M., van den Broeke, M., and Ettema, J.: Melting trends over the Greenland ice sheet (1958–2009) from spaceborne microwave data and regional climate models, The Cryosphere, 5, 359–375, doi:10.5194/tc-5-359-2011, 2011.

Fettweis, X., Franco, B., Tedesco, M., van Angelen, J. H., Lenaerts, J. T. M., van den Broeke, M. R., and Gallée, H.: Estimating the Greenland ice sheet surface mass

balance contribution to future sea level rise using the regional atmospheric climate model MAR, The Cryosphere, 7, 469–489, doi:10.5194/tc-7-469-2013, 2013.

Fowler, N. O., McCall, D., Chou, T. C., Holmes, J. C., and Hanenson, I. B.: Electrocardiographic changes and cardiac arrhythmias in patients receiving psychotropic drugs, Am. J. Cardiol., 37, 223–230, 1976.

Gallée, H.: Air–sea interactions over Terra Nova Bay during winter: simulation with a coupled atmosphere-polynya model, J. Geophys. Res., 102, 13835–13849, doi:10.1029/96JD03098, 1997.

Gallée, H. and Schayes, G.: Development of a three-dimensional meso-γ primitive equation model: katabatic winds simulation in the area of Terra Nova Bay, Antarctica, Mon. Weather Rev., 122, 671–685, doi:10.1175/1520-0493(1994)122<0671:DOATDM>2.0.CO;2, 1994.

Gubler, H. and Hiller, M.: The use of microwave FMCW radar in snow and avalanche research, Cold Reg. Sci. Technol., 9, 109–119, doi:10.1016/0165-232X(84)90003-X, 1984.

Hanna, E., Huybrechts, P., Cappelen, J., Steffen, K., Bales, R. C., Burgess, E., McConnell, J. R., Peder Steffensen, J., Van den Broeke, M., Wake, L., Bigg, G., Griffiths, M., and Savas, D.: Greenland Ice Sheet surface mass balance 1870 to 2010 based on Twentieth Century Reanalysis, and links with global climate forcing, J. Geophys. Res., 116, D24121, doi:10.1029/2011JD016387, 2011.

Hawley, R. L., Morris, E. M., Cullen, R., Nixdorf, U., Shepherd, A. P., and Wingham, D. J.: ASIRAS airborne radar resolves internal annual layers in the dry-snow zone of Greenland, Geophys. Res. Lett., 33, L04502, doi:10.1029/2005GL025147, 2006.

Hawley, R. L., Courville, Z. R., Kehrl, L. M., Lutz, E. R., Osterberg, E. C., Overly, T. B., and Wong, G. J.: Recent accumulation variability in northwest Greenland from ground-penetrating radar and shallow cores along the Greenland Inland Traverse, J. Glaciol., 60, 375–382, doi:10.3189/2014JoG13J141, 2014.

Kanagaratnam, P., Gogineni, S. P., Gundestrup, N., and Larsen, L.: High-resolution radar mapping of internal layers at the North Greenland Ice Core Project, J. Geophys. Res., 106, 33799, doi:10.1029/2001JD900191, 2001.

Kanagaratnam, P., Gogineni, S. P., Ramasami, V., and Braaten, D.: A wideband radar for high-resolution mapping of near-surface internal layers in glacial ice, IEEE T. Geosci. Remote, 42, 483–490, doi:10.1109/TGRS.2004.823451, 2004.

Koenig, L., Box, J., and Kurtz, N.: Improving surface mass balance over ice sheets and snow depth on sea ice, Eos Trans. AGU, 94, 100–100, doi:10.1002/2013EO100006, 2013.

Koenig, L., Forster, R., Brucker, L., and Miller, J.: Remote sensing of accumulation over the Greenland and Antarctic ice sheets, in: Remote Sensing of the Cryosphere, edited by: Tedesco, M., John Wiley & Sons, Ltd., Chichester, West Sussex, UK, 157–186, 2015.

Koenig, L. S., Miège, C., Forster, R. R., and Brucker, L.: Initial in situ measurements of perennial meltwater storage in the Greenland firn aquifer, Geophys. Res. Lett., 41, 2013GL058083, doi:10.1002/2013GL058083, 2014.

Koenig, L. and the Surface mass balance and snow on sea ice working group (SUMup): SUMup Snow Density Dataset, Greenbelt, MD, USA: NASA Goddard Space Flight Center, Digital media, http://neptune.gsfc.nasa.gov/csb/index.php?section=267 2015.

Krabill, W., Hanna, E., Huybrechts, P., Abdalati, W., Cappelen, J., Csatho, B., Frederick, E., Manizade, S., Martin, C., Sonntag, J., Swift, R., Thomas, R., and Yungel, J.: Greenland Ice Sheet: increased coastal thinning, Geophys. Res. Lett., 31, L24402, doi:10.1029/2004GL021533, 2004.

Lefebre, F.: Modeling of snow and ice melt at ETH Camp (West Greenland): a study of surface albedo, J. Geophys. Res., 108, 4231, doi:10.1029/2001JD001160, 2003.

Legarsky, J. J.: Synthetic-Aperture Radar (SAR) Processing of Glacial Ice Depth-Sounding Data, ka-Band Backscattering Measurements and Applications, PhD thesis, Retrieved from ProQuest Dissertations Publishing, 9946109, Lawrence, University of Kansas, KS, USA, 1999.

Leuschen, C.: IceBridge Snow Radar L1B Geolocated Radar Echo Strength Profiles, Boulder, Colorado, NASA DAAC at the National Snow and Ice Data Center, doi:10.5067/FAZTWP500V70, 2014.

Looyenga, H.: Dielectric constants of heterogeneous mixtures, Physica, 31, 401–406, doi:10.1016/0031-8914(65)90045-5, 1965.

MacGregor, J. A., Fahnestock, M. A., Catania, G. A., Paden, J. D., Prasad Gogineni, S., Young, S. K., Rybarski, S. C., Mabrey, A. N., Wagman, B. M., and Morlighem, M.: Radiostratigraphy and age structure of the Greenland Ice Sheet, J. Geophys. Res.-Earth, 120, 2014JF003215, doi:10.1002/2014JF003215, 2015.

Marshall, H.-P. and Koh, G.: FMCW radars for snow research, Cold Reg. Sci. Technol., 52, 118–131, 2008.

Medley, B., Joughin, I., Das, S. B., Steig, E. J., Conway, H., Gogineni, S., Criscitiello, A. S., McConnell, J. R., Smith, B. E., van den Broeke, M. R., Lenaerts, J. T. M., Bromwich, D. H., and Nicolas, J. P.: Airborne-radar and ice-core observations of annual snow accumulation

over Thwaites Glacier, West Antarctica confirm the spatiotemporal variability of global and regional atmospheric models, Geophys. Res. Lett., 40, 3649–3654, doi:10.1002/grl.50706, 2013.

Miège, C., Forster, R. R., Box, J. E., Burgess, E. W., McConnell, J. R., Pasteris, D. R., and Spikes, V. B.: Southeast Greenland high accumulation rates derived from firn cores and ground-penetrating radar, Ann. Glaciol., 54, 322–332, doi:10.3189/2013AoG63A358, 2013.

Mosley-Thompson, E., McConnell, J. R., Bales, R. C., Li, Z., Lin, P.-N., Steffen, K., Thompson, L. G., Edwards, R., and Bathke, D.: Local to regional-scale variability of annual net accumulation on the Greenland ice sheet from PARCA cores, J. Geophys. Res., 106, 33839–33851, doi:10.1029/2001JD900067, 2001.

Müller, K., Sinisalo, A., Anschütz, H., Hamran, S.-E., Hagen, J.-O., McConnell, J. R., and Pasteris, D. R.: An 860 km surface mass-balance profile on the East Antarctic plateau derived by GPR, Ann. Glaciol., 51, 1–8, doi:10.3189/172756410791392718, 2010.

Nghiem, S. V., Steffen, K., Neumann, G., and Huff, R.: Mapping of ice layer extent and snow accumulation in the percolation zone of the Greenland ice sheet, J. Geophys. Res., 110, F02017, doi:10.1029/2004JF000234, 2005.

Onana, V., Koenig, L. S., Ruth, J., Studinger, M., and Harbeck, J. P.: A semiautomated multilayer picking algorithm for ice-sheet radar echograms applied to ground-based near-surface data, IEEE T. Geosci. Remote, 53, 51–69, doi:10.1109/TGRS.2014.2318208, 2015.

Panzer, B., Gomez-Garcia, D., Leuschen, C., Paden, J., Rodriguez-Morales, F., Patel, A., Markus, T., Holt, B., and Gogineni, P.: An ultra-wideband, microwave radar for measuring snow thickness on sea ice and mapping near-surface internal layers in polar firn, J. Glaciol., 59, 244–254, doi:10.3189/2013JoG12J128, 2013.

Rodriguez-Morales, F., Gogineni, S., Leuschen, C. J., Paden, J. D., Li, J., Lewis, C. C., Panzer, B., Gomez-Garcia Alvestegui, D., Patel, A., Byers, K., Crowe, R., Player, K., Hale, R. D., Arnold, E. J., Smith, L., Gifford, C. M., Braaten, D., and Panton, C.: Advanced multifrequency radar instrumentation for polar research, IEEE T. Geosci. Remote, 52, 2824–2842, doi:10.1109/TGRS.2013.2266415, 2014.

Schneebeli, M., Coléou, C., Touvier, F., and Lesaffre, B.: Measurement of density and wetness in snow using time-domain reflectometry, Ann. Glaciol., 26, 69–72, 1998.

Shepherd, A., Ivins, E. R., A, G., Barletta, V. R., Bentley, M. J., Bettadpur, S., Briggs, K. H., Bromwich, D. H., Forsberg, R., Galin, N., Horwath, M., Jacobs, S., Joughin, I., King, M. A., Lenaerts, J. T. M., Li, J., Ligtenberg, S. R. M., Luckman, A., Luthcke, S. B., McMillan, M.,

Meister, R., Milne, G., Mouginot, J., Muir, A., Nicolas, J. P., Paden, J., Payne, A. J., Pritchard, H., Rignot, E., Rott, H., Sørensen, L. S., Scambos, T. A., Scheuchl, B., Schrama, E. J. O., Smith, B., Sundal, A. V., van Angelen, J. H., van de Berg, W. J., van den Broeke, M. R., Vaughan, D. G., Velicogna, I., Wahr, J., Whitehouse, P. L., Wingham, D. J., Yi, D., Young, D., and Zwally, H. J.: A reconciled estimate of ice-sheet mass balance, Science, 338, 1183–1189, doi:10.1126/science.1228102, 2012.

Spikes, V. B., Hamilton, G. S., Arcone, S. A., Kaspari, S., and Mayewski, P. A.: Variability in accumulation rates from GPR profiling on the West Antarctic plateau, Ann. Glaciol., 39, 238–244, doi:10.3189/172756404781814393, 2004.

Tiuri, M. E., Sihvola, A. H., Nyfors, E., and Hallikaiken, M.: The complex dielectric constant of snow at microwave frequencies, IEEE J. Oceanic Eng., 9, 377–382, doi:10.1109/JOE.1984.1145645, 1984.

van den Broeke, M., Bamber, J., Ettema, J., Rignot, E., Schrama, E., van de Berg, W. J., van Meijgaard, E., Velicogna, I., and Wouters, B.: Partitioning recent Greenland mass loss, Science, 326, 984–986, doi:10.1126/science.1178176, 2009.

Vernon, C. L., Bamber, J. L., Box, J. E., van den Broeke, M. R., Fettweis, X., Hanna, E., and Huybrechts, P.: Surface mass balance model intercomparison for the Greenland ice sheet, The Cryosphere, 7, 599–614, doi:10.5194/tc-7-599-2013, 2013.

Wiesmann, A. and Mätzler, C.: Microwave emission model of layered snowpacks, Remote Sens. Environ., 70, 307–316, doi:10.1016/S0034-4257(99)00046-2, 1999.

Table 1. Radar-derived accumulation-rate crossover analysis. Columns include the year the radar data were collected, the number of, the mean, the standard deviation and the maximum difference of radar-derived accumulation at crossover points. Minimum crossover values were zero for all years. The final column shows the mean difference between the gridded-radar-derived accumulation and the MAR estimates of accumulation.

Year	# of Crossovers	Mean Crossover (m w.e.)	Std. Crossover (m w.e.)	Max Crossovers (m w.e.)	Mean Difference Radar-MAR (m w.e.)
2009	21	0.03	0.04	0.12	−0.05
2010	270	0.02	0.02	0.16	−0.18
2011	992	0.04	0.06	0.60	0.01
2012	579	0.04	0.04	0.31	0.03

Figure 1. Locations of snow/firn density measurements (red circles) and ice core accumulation measurements (blue circles) used in this study with OIB flightline coverage from 2009 through 2012 (gray lines). Camp Century (CC) and NEEM core locations are labeled.

Figure 2. Mean observed (blue) and MAR modelled (red) densities profiles with one standard deviation (shaded regions) showing an underestimation of modelled densities in the top 1 m of snow/firn. The mean observed density in the top 1 m (green) was used with the modelled densities below to create a hybrid measured–modelled density profile. The locations of the density measurements are shown in Fig. 1.

Figure 3. Example Snow Radar echograms from 2011 in the percolation zone (top), inland from Jakobshavn Isbræ, and dry snow zone (bottom), near the ice divide ~ 220 km south of Summit Station, showing automatically picked layers (black) resulting from the layer picking algorithm before any manual adjustments. Indexing by year is shown at the left end of each picked layer. Snow Radar data frames represented are 20 110 422_01_218 to 20 110 422_01_244 (top) and 20 110 426_03_155 to 20 110 426_03_180 (bottom) (Leuschen, 2014).
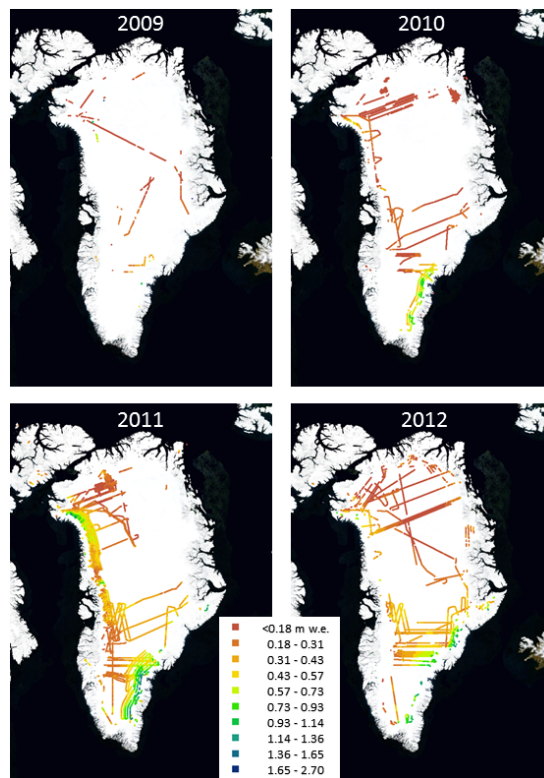
Figure 4. Radar-derived-annual accumulation rate (m w.e.) for 2009 through 2012 from Operation IceBridge Snow Radar data.
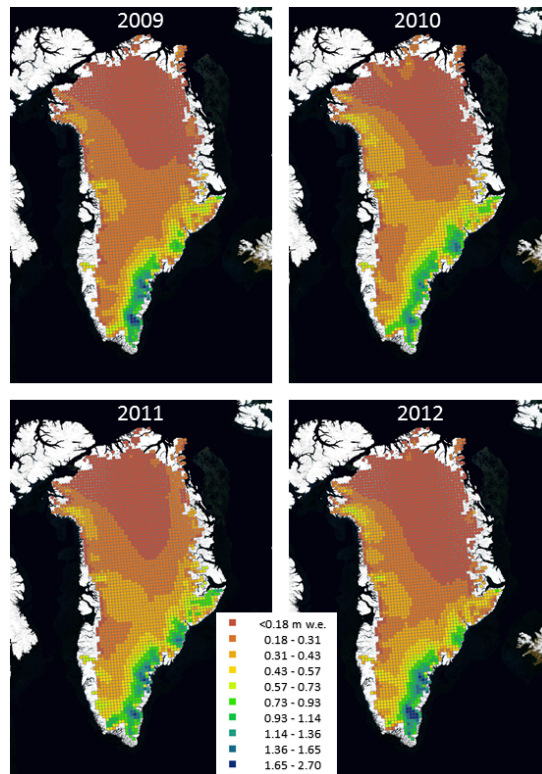
Figure 5. Modelled estimates of annual accumulation (m w.e.) over the GrIS for 2009 through 2012 from the Modèle Atmosphérique Régional (MAR) regional climate model (v3.5.2).
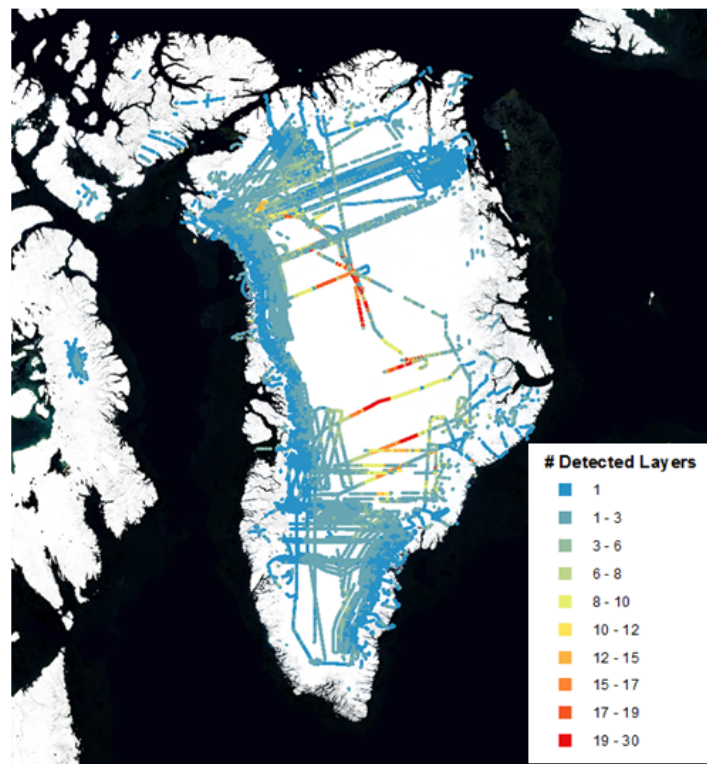
Figure 6. Number of detected annual layers from 2009 through 2012 showing that, for the majority of the GrIS, less than three layers, or previous years of accumulation, were detected.
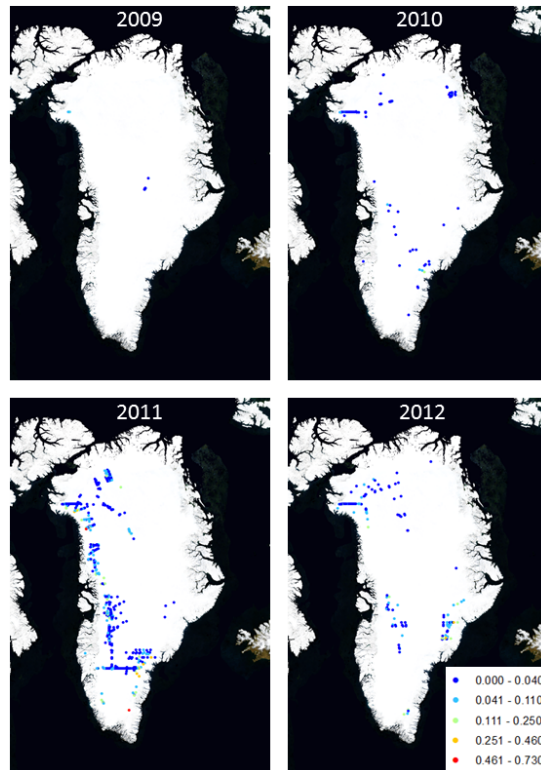
Figure 7. Maps of annual-crossover error (m w.e.) from the radar-derived accumulation for 2009 through 2012.
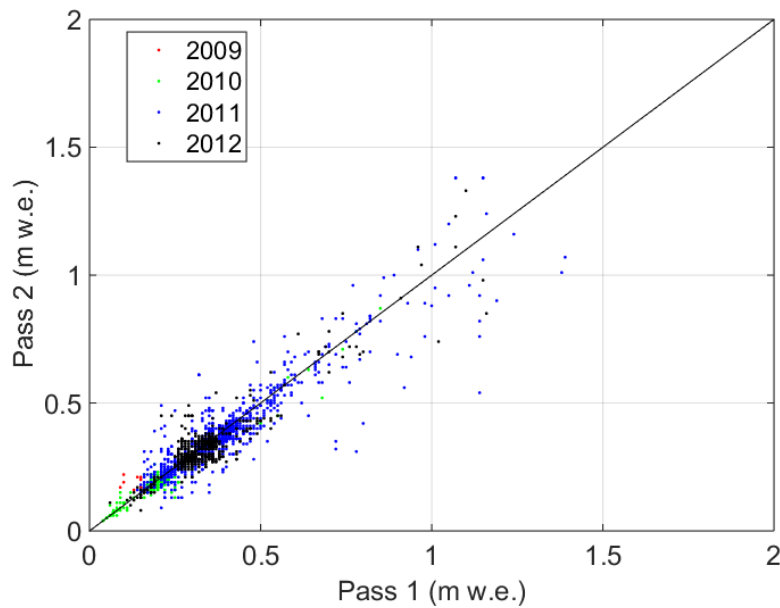
Figure 8. Crossover errors from the radar-derived accumulation (m w.e.) from 2009 through 2012. Figure 7 shows the spatial distribution of these crossover errors.
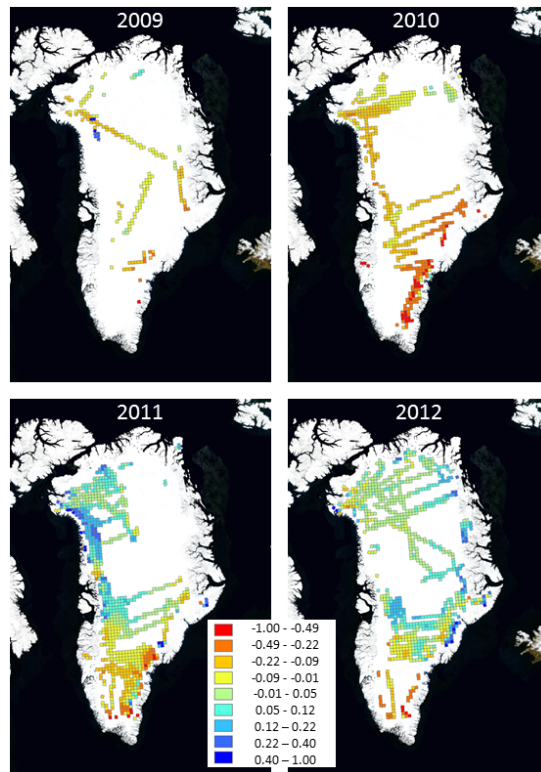
Figure 9. Difference between annual radar-derived and MAR-estimated accumulation (m w.e.) showing MAR overestimation in red and underestimation in blue.
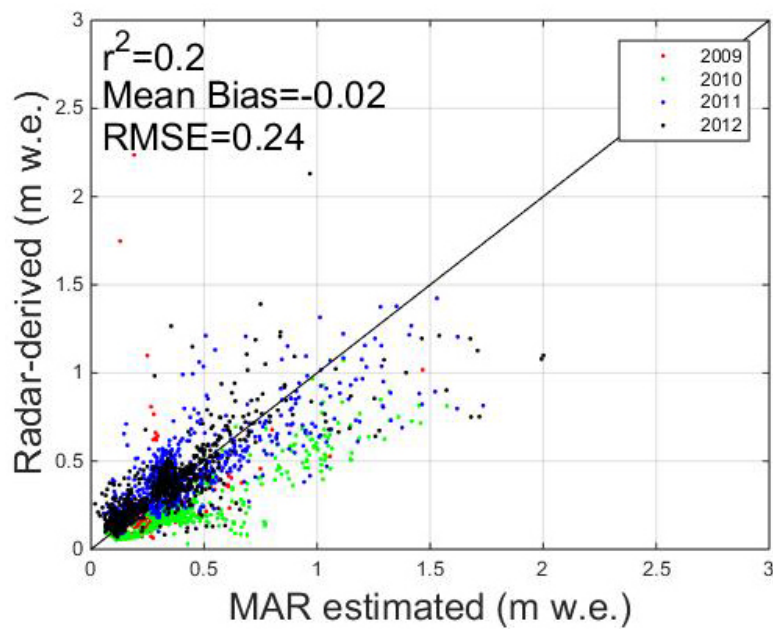
Figure 10. Comparison between radar-derived and MAR-estimated accumulation (m w.e.). Radar-derived accumulations (Fig. 4) were averaged within each MAR grid cell. Figure 9 shows the spatial distribution of the differences.
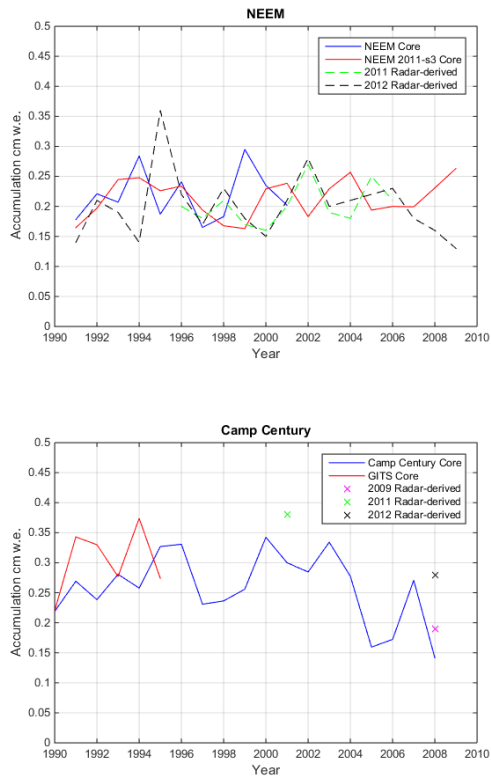
Figure 11. Annual accumulation rate measured from the two cores at both the NEEM and Camp Century locations compared to temporally overlapping radar-derived values.

6731